

Optimal efficiency and power, and their trade-off in three-terminal quantum thermoelectric engines with two output electric currents

Jincheng Lu,¹ Yefeng Liu,¹ Rongqian Wang,¹ Chen Wang,² and Jian-Hua Jiang^{1,*}

¹*School of Physical Science and Technology & Collaborative Innovation Center of Suzhou Nano Science and Technology, Soochow University, Suzhou 215006, China*

²*Department of Physics, Zhejiang Normal University, Jinhua, Zhejiang 321004, China*

 (Received 27 May 2019; revised manuscript received 18 September 2019; published 30 September 2019)

We establish a theory of maximal energy efficiency and output power for three-terminal thermoelectric engines which have two independent output electric currents and one input heat current. This setup goes beyond conventional heat engines with only one output electric current. We derive the maximal energy efficiency and output power and their trade-off for three-terminal thermoelectric engines with and without time-reversal symmetry. This formalism goes beyond the known results for conventional thermoelectric engines and shows some interesting features. A concrete example of a quantum-dot three-terminal thermoelectric engine is studied to demonstrate that for the same system, our setup can substantially enlarge the physical parameter region with high efficiency and power, when compared with previous setups with only one output electric current. Therefore, the setup with two output electric currents offers a promising pathway toward high-performance thermoelectric devices. Our theoretical framework also applies for thermoelectric heat engines with multiple output electric currents, providing a formalism for the study of maximal efficiency and power in complex thermoelectric materials and devices.

DOI: [10.1103/PhysRevB.100.115438](https://doi.org/10.1103/PhysRevB.100.115438)

I. INTRODUCTION

Thermoelectric phenomena have attracted lots of research interest because of their relevance to fundamental physics and state-of-the-art energy applications [1–6]. The understanding of fundamental thermodynamic constraints on the efficiency and power of nanoscale thermoelectric devices has been a subject of widespread interest in the past decades [7–17]. Recent theoretical [7–37] and experimental [38–42] studies on thermoelectric phenomena in mesoscopic systems have renewed the fundamental understanding on thermoelectric transport and energy conversion. Several concepts, such as reversible thermoelectric energy conversion [43,44], inelastic thermoelectric transport [5,18–25], fundamental bounds on the maximal energy efficiency and output power [7–10,16,17,45], universal fluctuations of energy efficiency [11–13,15], cooperative thermoelectric effects [8,46,47], and nonlinear thermoelectric effects [48] were proposed. In particular, with the seminal works by Benenti *et al.* [49] and later by Brandner *et al.* [50], mesoscopic thermoelectric heat engines with broken time-reversal symmetry have gained much interest, particularly in multiterminal transport configurations [6,29,51–55] where thermoelectric engines with asymmetric Onsager transport coefficients are studied in the setup with one input heat current and one output electric current.

In the linear-response regime, the transport properties of thermoelectric engines studied in the literature are described

by the following equation,

$$\begin{pmatrix} I_e \\ I_Q \end{pmatrix} = \begin{pmatrix} G & L_1 \\ L_2 & K \end{pmatrix} \begin{pmatrix} V \\ \frac{T_h - T_c}{T_h} \end{pmatrix}, \quad (1)$$

where I_e and I_Q are the charge and heat currents, and G and K are the charge and heat conductivities, respectively. L_1 and L_2 describe the Seebeck and Peltier effects, separately. V is the voltage bias across the device, and T_h and T_c are the temperatures of the hot and cold thermal reservoirs, respectively. In time-reversal broken multiterminal systems the two coefficients L_1 and L_2 can be different [29,49], though they are identical for time-reversal symmetric thermoelectric devices in the linear-transport regime. The energy efficiency for thermoelectric heat engines is defined as $\eta = -I_e V / I_Q$ with $I_e V < 0$ (i.e., power output) and $I_Q > 0$ (i.e., heat consumption). As shown in Ref. [49], for a thermoelectric heat engine described by the above equation, the maximal energy efficiency and the energy efficiency at the maximal output power condition are given by

$$\eta_{\max} = \eta_C r_{12} \frac{\sqrt{ZT + 1} - 1}{\sqrt{ZT + 1} + 1}, \quad \eta(W_{\max}) = \frac{\eta_C}{2} \frac{r_{12} ZT}{2 + ZT}, \quad (2)$$

respectively, where $\eta_C = \frac{T_h - T_c}{T_h}$ is the Carnot efficiency and

$$ZT = \frac{L_1 L_2}{GK - L_1 L_2}, \quad r_{12} = \frac{L_1}{L_2} \quad (3)$$

are the thermoelectric figure of merit and the ratio between the two off-diagonal elements. For a time-reversal symmetric macroscopic system with length l and cross-section area \mathcal{A} , the above equations come back to the more familiar form, $r_{12} = 1$ and the figure of merit $ZT = \sigma S^2 T / \kappa$, where

*jianhua.jiang@suda.edu.cn

$\sigma = Gl/A$ is the electric conductivity, $S = L/(TG)$ is the Seebeck coefficient, and $\kappa = (K - L_1L_2/G)l/(AT)$ is the thermal conductivity. Benenti *et al.* [49] showed that the above results give guidance to exceed the so-called Curzon-Ahborn limit [56] η_{CA} for the energy efficiency at maximal output power (in the linear-response regime, $\eta_{CA} = \eta_C/2$).

The existing studies on three-terminal thermoelectric energy conversion are restricted to the situation with only one output electric current (i.e., the charge and heat currents flowing out of the third terminal are set to zero) [53,54]. Even for multiterminal systems, electric (heat) currents except one are suppressed by tuning the electrochemical potentials and temperatures of the other electrodes [29]. Such constraints are not easy to realize in experiments. Besides, they may be disadvantageous for the performance of the thermoelectric heat engine, as shown by the numerical calculations in this paper.

The main purpose of this paper is to search for high-performance thermoelectric energy conversion in the largely unexplored regime where thermoelectric engines have more than one output electric current. For this purpose, we develop a theoretical framework to calculate the maximal energy efficiency and output power for thermoelectric engines with multiple output electric currents. Such thermoelectric engines can be feasibly realized in multiterminal mesoscopic systems connected to two heat baths. To be concrete, we study a setup for a three-terminal thermoelectric engine where one electrode is attached to the hot thermal reservoir, and the other two electrodes are attached to the same cold thermal reservoir (see Fig. 1). No further constraints are imposed on the device which acts as a thermoelectric engine with two output electric currents. This setup is more feasible to realize than previous three-terminal setups with only one output electric current. We find that such a setup can substantially enlarge the physical parameter region with high-energy efficiency and output power. We also find situations where both the efficiency and power can be considerably increased when the three-

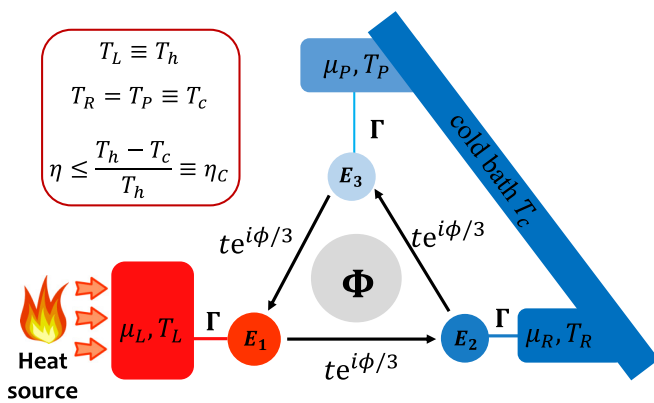


FIG. 1. Schematic of a quantum-dot thermoelectric heat engine with a magnetic flux Φ . Three quantum dots (with energy E_i , $i = L, R, P$) are connected to three electrodes. The tunneling rate between the dots and the electrodes is Γ . We consider the setup where both the R and P electrodes are connected to a cold reservoir of temperature T_c , whereas the L electrode is connected to a hot reservoir of temperature T_h .

terminal thermoelectric engine goes from the previous setup to the present setup. We derive the analytical expressions for maximal energy efficiency and output power for the present setup and find their trade-off relations [8,9,16,17,53] in the linear-response regime. We clarify the physical interpretation of the output electric power and how to exploit it, when the thermoelectric engine has two output electric currents. Our theoretical framework can also be applied to thermoelectric engines with multiple output electric currents, providing a pathway toward multiterminal thermoelectric devices with multiple electric currents which are distinct from previous setups with only one electric current.

This paper is organized as follows. In Sec. II, we introduce the three-terminal thermoelectric transport model. In Sec. III, we obtain the maximal energy efficiency and output power, and derive the relations between the maximum efficiency, the maximum power, the efficiency at maximal power, and the power at maximal efficiency in linear response. In Sec. IV, we deduce the bounds on the maximal efficiency and power in the linear-response regime. In Sec. V, we analyze the efficiency and power of quantum-dot three-terminal thermoelectric engines with two output electric currents. In particular, the advantages of the setup with two output electric currents are emphasized. We conclude and remark for future studies in Sec. VI.

II. MESOSCOPIC THREE-TERMINAL QUANTUM-DOT THERMOELECTRIC HEAT ENGINES

As shown in Fig. 1, we consider a mesoscopic thermoelectric device consisting of three quantum dots (QDs) coupled to three electrodes. This is a minimal model to demonstrate the setup with two output electric currents. Although this model has been studied before [29,51,52,54], the configuration illustrated in Fig. 1 has yet to be studied. This model is valid when the Coulomb interaction can be neglected [51]. Each QD is coupled to the nearby electrode. We thus may employ the indices 1/2/3 to label the leads $L/R/P$, respectively [13].

Hopping between QDs is affected by the magnetic flux Φ piercing through the device at the center with the phase $\phi/3$ assigned to each of the hoppings ($\phi = 2\pi\Phi/\Phi_0$, where Φ_0 is flux quantum). The system is described by the following Hamiltonian [51],

$$\hat{H} = \hat{H}_{\text{qd}} + \hat{H}_{\text{lead}} + \hat{H}_{\text{tun}}, \quad (4)$$

where

$$\hat{H}_{\text{qd}} = \sum_{i=1,2,3} E_i d_i^\dagger d_i + (te^{i\phi/3} d_{i+1}^\dagger d_i + \text{H.c.}), \quad (5)$$

$$\hat{H}_{\text{lead}} = \sum_{i=1,2,3} \sum_k \varepsilon_k c_{ik}^\dagger c_{ik}, \quad (6)$$

$$\hat{H}_{\text{tun}} = \sum_{i,k} V_{ik} d_i^\dagger c_{ik} + \text{H.c.} \quad (7)$$

Here, d_i^\dagger and d_i create and annihilate an electron in the i th QD with an energy E_i , respectively, and t is the tunneling amplitude between the QDs. c_{ik}^\dagger and c_{ik} create and annihilate an electron in the i th electrode with the energy E_i ($i = 1, 2, 3$).

The chemical potentials and temperatures of three reservoirs are denoted by μ_i and T_i ($i = L, R, P$), respectively. For

each reservoir, there are electric and heat currents flowing out of the reservoir. In total there are six currents. However, only four of them are independent, due to charge and energy conservation [51]. We choose the charge and heat currents flowing out of the L and P reservoirs as the independent currents which are denoted as I_e^i and I_Q^i ($i = L, P$), respectively. The corresponding thermodynamic forces are

$$F_e^i = \frac{\mu_i - \mu_R}{e}, \quad F_Q^i = \frac{T_i - T_R}{T_i} \quad (i = L, P), \quad (8)$$

where $e < 0$ is the electric charge. We focus on the setup where the L reservoir is connected to the hot bath and the R and P reservoirs are connected to the cold bath, i.e.,

$$T_L = T_h, \quad T_P = T_R = T_c. \quad (9)$$

There are two independent output electric currents, I_e^L and I_e^P (i.e., the charge currents flowing out of the L and P reservoirs), whereas there is only one input heat current $I_Q \equiv I_Q^L$ (i.e., the heat current flowing out of the hot reservoir L) with the corresponding force $F_Q \equiv F_Q^L$.

With such a setup, the phenomenological Onsager transport equation is written in the linear-response regime as

$$\begin{pmatrix} \vec{I}_e \\ I_Q \end{pmatrix} = \begin{pmatrix} \hat{\mathcal{M}}_{ee} & \hat{\mathcal{M}}_{eQ} \\ \hat{\mathcal{M}}_{Qe} & \mathcal{M}_{QQ} \end{pmatrix} \begin{pmatrix} \vec{F}_e \\ F_Q \end{pmatrix}, \quad (10)$$

where the symbols e and Q are used to abbreviate the indices of forces and currents for charge and heat, respectively [i.e., $\vec{I}_e = (I_e^L, I_e^P)^T$, $\vec{F}_e = (F_e^L, F_e^P)^T$, $I_Q \equiv I_Q^L$, and $F_Q \equiv F_Q^L$; here the superscript T stands for vector/matrix transpose]. $\hat{\mathcal{M}}_{ee}$ denotes the 2×2 charge conductivity tensor, the 2×1 matrix $\hat{\mathcal{M}}_{eQ}$ describes the Seebeck effect, while the matrix $\hat{\mathcal{M}}_{Qe}$ describes the Peltier effect. The 1×1 matrix (scalar) \mathcal{M}_{QQ} represents the heat conductivity. For systems with time-reversal symmetry (e.g., $\phi = 0, \pi$), Onsager's reciprocal relation gives $\hat{\mathcal{M}}_{eQ} = \hat{\mathcal{M}}_{Qe}^T$. In contrast, for time-reversal broken systems, they are not equal to each other.

Consider that the thermoelectric engine is giving electric power to two energy storage capacitors. One of them (connected with the L and R electrodes) has a voltage bias $(\mu_L - \mu_R)/e$, while the other one (connected with the P and R electrodes) has a voltage bias $(\mu_P - \mu_R)/e$. Assuming the capacitances of these capacitors are very large (e.g., a large power grid or a high capacitance rechargeable battery), the output electric power of the thermoelectric engine is then [8]

$$W = -\vec{I}_e^T \vec{F}_e = -(\vec{F}_e^T \hat{\mathcal{M}}_{ee} \vec{F}_e + \vec{F}_e^T \hat{\mathcal{M}}_{eQ} F_Q). \quad (11)$$

The situation when the thermoelectric engine gives electric power to a resistor circuit will be discussed at the end of this paper. We the present situation where the energy efficiency is defined as

$$\eta = \frac{W}{I_Q} = -\frac{\vec{F}_e^T \hat{\mathcal{M}}_{ee} \vec{F}_e + \vec{F}_e^T \hat{\mathcal{M}}_{eQ} F_Q}{\hat{\mathcal{M}}_{Qe} \vec{F}_e + \mathcal{M}_{QQ} F_Q} \leq \eta_C. \quad (12)$$

Here, $\eta_C = 1 - T_c/T_h = \mathcal{F}_Q$ is the Carnot efficiency which is the absolute upper bound for the attainable energy efficiency due to the second law of thermodynamics.

III. MAXIMAL ENERGY EFFICIENCY AND OUTPUT POWER AND THEIR TRADE-OFF

We note that in the linear-response regime the energy efficiency is invariant under the scaling transformation $\vec{F}_e \rightarrow a\vec{F}_e$ and $F_Q \rightarrow aF_Q$, with a being an arbitrary constant. In comparison, the output power scales as $W \rightarrow a^2W$. We can then fix F_Q and obtain the maximal energy efficiency by solving the following differential equation,

$$\frac{\partial \eta}{\partial \vec{F}_e} = 0. \quad (13)$$

We obtain that

$$\vec{F}_e = -\frac{1}{2} [\eta_{\max} (\hat{\mathcal{M}}_{ee})^{-1} \hat{\mathcal{M}}_{Qe}^T F_Q + (\hat{\mathcal{M}}_{ee})^{-1} \hat{\mathcal{M}}_{eQ} F_Q]. \quad (14)$$

Here, we define

$$\overline{\hat{\mathcal{M}}_{ee}} \equiv \frac{1}{2} (\hat{\mathcal{M}}_{ee} + \hat{\mathcal{M}}_{ee}^T) \quad (15)$$

as the symmetric charge conductivity tensor. Inserting Eq. (14) into Eq. (12), we arrive at

$$\eta_{\max} = \eta_C \frac{\lambda_1 - \lambda_2 (\eta_{\max}/\eta_C)^2}{4 - 2[\lambda_2 (\eta_{\max}/\eta_C) + \lambda_3]}. \quad (16)$$

Solving the above quadratic equation, we obtain the maximal efficiency as

$$\eta_{\max} = \eta_C \frac{2 - \lambda_3 - \sqrt{(2 - \lambda_3)^2 - \lambda_1 \lambda_2}}{\lambda_2}. \quad (17)$$

Here,

$$\lambda_1 \equiv \hat{\mathcal{M}}_{eQ}^T (\overline{\hat{\mathcal{M}}_{ee}})^{-1} \hat{\mathcal{M}}_{eQ} \mathcal{M}_{QQ}^{-1}, \quad (18a)$$

$$\lambda_2 \equiv \hat{\mathcal{M}}_{Qe} (\overline{\hat{\mathcal{M}}_{ee}})^{-1} \hat{\mathcal{M}}_{Qe}^T \mathcal{M}_{QQ}^{-1}, \quad (18b)$$

$$\lambda_3 \equiv \hat{\mathcal{M}}_{Qe} (\overline{\hat{\mathcal{M}}_{ee}})^{-1} \hat{\mathcal{M}}_{eQ} \mathcal{M}_{QQ}^{-1} \quad (18c)$$

are three dimensionless parameters that characterize the thermoelectric transport properties of the system. The output power at maximum efficiency is

$$W(\eta_{\max}) = W_0 \left[\lambda_1 - \lambda_2 \left(\frac{\eta_{\max}}{\eta_C} \right)^2 \right], \quad W_0 \equiv \frac{1}{4} \mathcal{M}_{Qe} F_Q^2. \quad (19)$$

Similarly, we can obtain the maximal output power with fixed F_Q by solving the following equation,

$$\frac{\partial W}{\partial \vec{F}_e} = 0, \quad (20)$$

which yields

$$W_{\max} = \lambda_1 W_0. \quad (21)$$

Meanwhile, the efficiency at maximum output power is [57,58]

$$\eta(W_{\max}) = \eta_C \frac{\lambda_1}{4 - 2\lambda_3}. \quad (22)$$

Comparing the energy efficiency and output power for the above two optimization schemes, we find that

$$\frac{\eta_{\max}}{\eta(W_{\max})} = 1 + \frac{\lambda_2}{\lambda_1} \left(\frac{\eta_{\max}}{\eta_C} \right)^2 \quad (23)$$

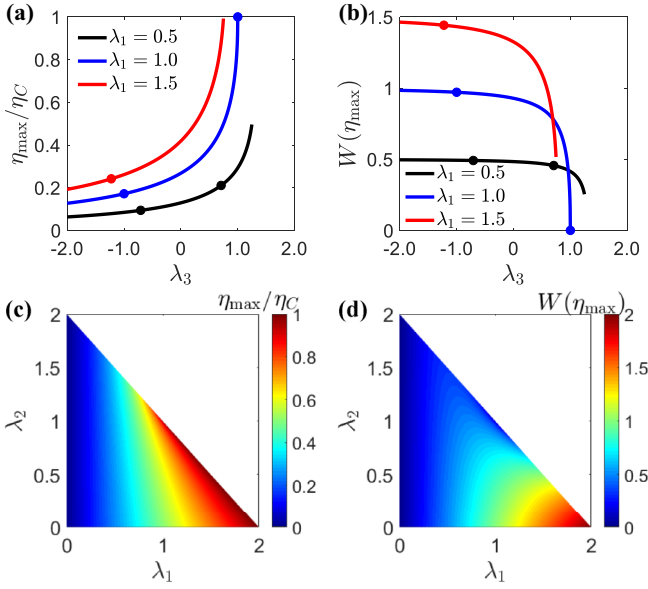


FIG. 2. (a) η_{\max}/η_C and (b) $W(\eta_{\max})$ as functions of λ_3 for different λ_1 , when $\lambda_2 = 1$. The black dots represent the limit given by Eq. (29). (c) η_{\max} and (d) $\eta(W_{\max})$ as functions of λ_1 and λ_2 when $\lambda_3 = 1$. The white region is forbidden due to the second law of thermodynamics. The unit of the output power is W_0 .

and

$$\frac{W(\eta_{\max})}{W_{\max}} = 1 - \frac{\lambda_2}{\lambda_1} \left(\frac{\eta_{\max}}{\eta_C} \right)^2. \quad (24)$$

The above trade-off relations between the optimization of the efficiency and power are presented graphically in Fig. 2. These relations also reveal several important properties: First, the performance of the thermoelectric engine is better when $\lambda_2 < \lambda_1$ compared with the situation with $\lambda_2 > \lambda_1$. In addition, when $\lambda_2 < \lambda_1$, the efficiency at maximal output power can possibly exceed the Curzon-Ahlborn limit [55] in the linear response $\eta_{CA} = \eta_C/2$, in consistency with previous works [29,49,50]. In the previous setups, it is known that the second law of thermodynamics alone allows a finite power output at Carnot efficiency. In our system the second law of thermodynamics alone also allows this situation when $\lambda_1 > \lambda_2$. However, most microscopic theories of transport (such as the scattering theory used below [9,10,50]) have zero power output at Carnot efficiency, so the possibility of finite power output at Carnot efficiency remains under debate [9,10,27–29,49,50,59–63].

We now make two remarks. First, the above results are also valid for the situation with multiple (>2) output electric currents. This can be readily verified through the vectorial (matrix) formulation used in the above discussions. Second, the second law of thermodynamics imposes the following constraints on the dimensionless parameters,

$$\lambda_1 \geq 0, \quad \lambda_2 \geq 0, \quad \lambda_1 + \lambda_2 + 2\lambda_3 \leq 4. \quad (25)$$

The derivation of the above constraints goes as follows: The entropy production rate associated with the thermoelectric

transport is given by [7]

$$\begin{aligned} T_R \dot{S} &= \vec{I}_e^T \vec{F}_e + I_Q F_Q \\ &= (\vec{F}_e, F_Q) \begin{pmatrix} \hat{\mathcal{M}}_{ee} & \hat{\mathcal{M}}_{eQ} \\ \hat{\mathcal{M}}_{Qe} & \mathcal{M}_{QQ} \end{pmatrix} \begin{pmatrix} \vec{F}_e \\ F_Q \end{pmatrix}. \end{aligned} \quad (26)$$

The second law of thermodynamics requires $\dot{S} \geq 0$ for all values of \vec{F}_e and F_Q , which is equivalent to require the following matrix to be positive semidefinite,

$$\begin{pmatrix} \overline{\hat{\mathcal{M}}_{ee}} & \frac{\hat{\mathcal{M}}_{eQ}^T + \hat{\mathcal{M}}_{Qe}}{2} \\ \frac{\hat{\mathcal{M}}_{Qe}^T + \hat{\mathcal{M}}_{eQ}}{2} & \mathcal{M}_{QQ} \end{pmatrix}. \quad (27)$$

Therefore, $\mathcal{M}_{QQ} \geq 0$ and the matrix $\overline{\hat{\mathcal{M}}_{ee}}$ is positive semidefinite. In addition, the determinant of the above matrix is positive semidefinite which yields

$$|\overline{\hat{\mathcal{M}}_{ee}}| \left| \mathcal{M}_{QQ} - \frac{\hat{\mathcal{M}}_{eQ}^T + \hat{\mathcal{M}}_{Qe}}{2} (\overline{\hat{\mathcal{M}}_{ee}})^{-1} \frac{\hat{\mathcal{M}}_{Qe}^T + \hat{\mathcal{M}}_{eQ}}{2} \right| \geq 0, \quad (28)$$

where $||$ is the determinant of the matrix. From these positive semidefinite properties, one can deduce Eq. (25) straightforwardly.

We now compare our formalism with previous formalisms. In the previous studies, the charge and heat currents flowing out of the P terminal are tuned to vanish by adjusting the chemical potential and temperature at the P terminal (often called a probe terminal in mesoscopic physics). Under such constraints (denoted as $P = 0$ for short throughout this paper), there is only one heat current and one electric current in the system. Thermoelectric transport is then described by a 2×2 Onsager matrix [6,29,51–54]. In this limit, the matrices $\hat{\mathcal{M}}_{ee}$, $\hat{\mathcal{M}}_{eQ}$, and $\hat{\mathcal{M}}_{Qe}$ become scalar quantities. From the definition in Eq. (18), one finds that for such a setup

$$\lambda_3^2 = \lambda_1 \lambda_2, \quad \text{for } P = 0. \quad (29)$$

The above constraint describes one of the main differences between our formalism and the previous formalisms. The other major difference is that the temperatures of the P and R terminals are identical in our setup, whereas they are generally different in previous formalisms. As shown in Fig. 2(a), for the same physical parameters (e.g., the same device), our setup may yield higher-energy efficiency. In the figure, the black dot represents the limit (29) considered in previous studies. Figure 2(b) shows that larger output power may also be achieved. The opposite trends of energy efficiency and output power with λ_3 is a reflection of the efficiency-power trade-off. Figures 2(c) and 2(d) show the maximal energy efficiency and the output power at such an efficiency. These results show again that the region with $\lambda_1 > \lambda_2$ is more favorable than the region with $\lambda_1 < \lambda_2$ for thermoelectric heat engine.

IV. THERMODYNAMIC BOUNDS ON THE EFFICIENCY AND POWER IN THE LINEAR-TRANSPORT REGIME

The thermodynamic bounds on the maximal energy efficiency η_{\max} and the energy efficiency at the maximum output power $\eta(W_{\max})$ can be reached at the reversible limit where

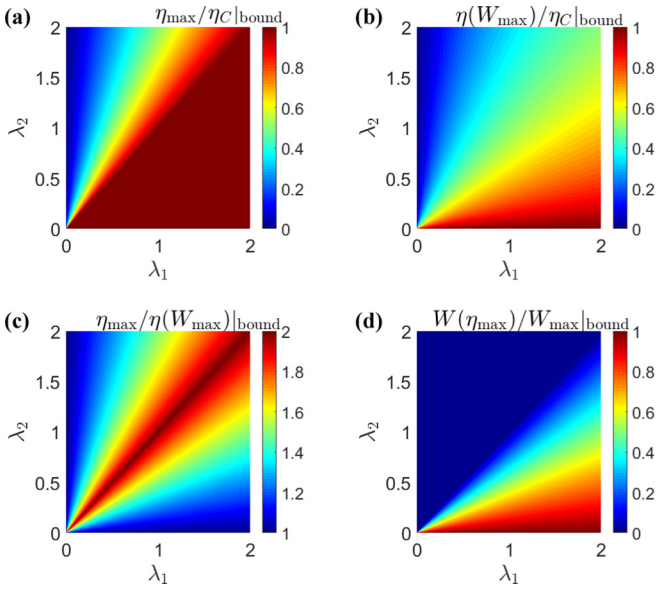


FIG. 3. Bounds on (a) the maximum energy efficiency, $\eta_{\max}|_{\text{bound}}$, (b) the efficiency at the maximum output power, $\eta(W_{\max})|_{\text{bound}}$, (c) the ratio between efficiency, $\eta_{\max}/\eta(W_{\max})|_{\text{bound}}$, and (d) the ratio between power, $W(\eta_{\max})/W_{\max}|_{\text{bound}}$, as functions of λ_1 and λ_2 .

$\lambda_1 + \lambda_2 + 2\lambda_3 = 4$, leading to

$$\eta_{\max}|_{\text{bound}} = \begin{cases} \eta_C \frac{\lambda_1}{\lambda_2}, & \text{if } \lambda_1 < \lambda_2, \\ \eta_C, & \text{if } \lambda_1 \geq \lambda_2. \end{cases} \quad (30)$$

The above results are presented graphically in Fig. 3(a) for various λ_1 and λ_2 . The upper bound for the efficiency at the maximum output power is

$$\eta(W_{\max})|_{\text{bound}} = \eta_C \frac{\lambda_1}{\lambda_1 + \lambda_2}. \quad (31)$$

From the above, the Curzon-Ahlborn limit [55,64] for the energy efficiency at the maximum output power condition, $\eta_{\text{CA}} = \eta_C/2$, can in principle be overcome for $\lambda_1 > \lambda_2$. This observation is consistent with previous studies [6,29,49–54] (in particular, the seminal work by Benenti *et al.* [49]). We remark that although the above formalism, as previous formalisms [6,49,51], allow an access of Carnot efficiency at finite power, microscopic mechanisms may forbid such situations, as shown in Refs. [27–29,50].

Combining Eqs. (30) and (31), we find the ratio between those bounds on the energy efficiency,

$$\left. \frac{\eta_{\max}}{\eta(W_{\max})} \right|_{\text{bound}} = \begin{cases} 1 + \frac{\lambda_1}{\lambda_2}, & \text{if } \lambda_1 < \lambda_2, \\ 1 + \frac{\lambda_2}{\lambda_1}, & \text{if } \lambda_1 \geq \lambda_2. \end{cases} \quad (32)$$

Meanwhile, the ratio between those bounds on the output power is given by

$$\left. \frac{W(\eta_{\max})}{W_{\max}} \right|_{\text{bound}} = \begin{cases} 1 - \frac{\lambda_1}{\lambda_2}, & \text{if } \lambda_1 < \lambda_2, \\ 1 - \frac{\lambda_2}{\lambda_1}, & \text{if } \lambda_1 \geq \lambda_2. \end{cases} \quad (33)$$

As presented in Figs. 3(c) and 3(d), the trade-off between the maximal energy efficiency and the maximal output power is substantially reduced when $\lambda_1 \gg \lambda_2$. Thus, in this regime high-energy efficiency and large output power may be obtained simultaneously.

V. LINEAR THERMOELECTRIC TRANSPORT COEFFICIENTS IN NONINTERACTING QUANTUM-DOT THREE-TERMINAL SYSTEMS

In this section, the thermoelectric transport properties of the quantum-dot three-terminal thermoelectric engine will be calculated using the Landauer-Büttiker formalism. The linear-transport properties of the three-terminal thermoelectric engine will be derived for the calculation of the maximum efficiency and power for the setup illustrated in Fig. 1. This model is utilized to compare concretely the performance of the three-terminal thermoelectric engines between the previous setup and the setup illustrated in Fig. 1. With the setup in Fig. 1, the linear thermoelectric transport is described by the following equation,

$$\begin{pmatrix} I_e^L \\ I_e^P \\ I_Q \end{pmatrix} = \begin{pmatrix} M_{11} & M_{12} & M_{13} \\ M_{21} & M_{22} & M_{23} \\ M_{31} & M_{32} & M_{33} \end{pmatrix} \begin{pmatrix} F_e^L \\ F_e^P \\ F_Q \end{pmatrix}. \quad (34)$$

The coherent flow of charge and heat through a noninteracting QD system can be described using the Landauer-Büttiker theory. The charge and heat currents flowing out of the left reservoir are given by [1,65]

$$I_e^L = \frac{2e}{h} \int dE \sum_i [\mathcal{T}_{iL}(E)f_L(E) - \mathcal{T}_{Li}(E)f_R(E)],$$

$$I_Q = \frac{2}{h} \int dE \sum_i (E - \mu_L) [\mathcal{T}_{iL}(E)f_L(E) - \mathcal{T}_{Li}(E)f_R(E)],$$

where $f_i(E) = \{\exp[(E - \mu_i)/k_B T_i] + 1\}^{-1}$ is the Fermi-Dirac distribution function and \mathcal{T}_{ij} is the transmission probability from terminal j to terminal i . Here, h is the Planck constant. The factor of 2 comes from the spin degeneracy of electrons. We assume that the magnetic flux is confined in a small region at the center of the device and the magnetic field is vanishing in regions with electrons. Consequently, the electron spin degeneracy is not lifted by the magnetic flux. An analogous expression can be written for I_e^P , provided that the subscript (superscript) L is substituted by P .

The Onsager coefficients M_{ij} are obtained from the linear expansion of the electric currents I_e^i ($i = L, P$) and the heat current I_Q in terms of the thermodynamic forces [1,65] F_e^i ($i = L, P$) and F_Q as follows,

$$M_{11} = \frac{2e^2}{hk_B T} \int_{-\infty}^{\infty} dE \sum_{i \neq L} \mathcal{T}_{Li}(E) F(E),$$

$$M_{12} = -\frac{2e^2}{hk_B T} \int_{-\infty}^{\infty} dE \mathcal{T}_{LP}(E) F(E),$$

$$M_{13} = M_{31} = \frac{2e}{hk_B T} \int_{-\infty}^{\infty} dE (E - \mu) \sum_{i \neq L} \mathcal{T}_{Li}(E) F(E),$$

$$\begin{aligned}
 M_{21} &= -\frac{2e^2}{\hbar k_B T} \int_{-\infty}^{\infty} dE \mathcal{T}_{PL}(E) F(E), \\
 M_{22} &= \frac{2e^2}{\hbar k_B T} \int_{-\infty}^{\infty} dE \sum_{i \neq P} \mathcal{T}_{Pi}(E) F(E), \\
 M_{23} &= -\frac{2e}{\hbar k_B T} \int_{-\infty}^{\infty} dE (E - \mu) \mathcal{T}_{PL}(E) F(E), \\
 M_{32} &= -\frac{2e}{\hbar k_B T} \int_{-\infty}^{\infty} dE (E - \mu) \mathcal{T}_{LP}(E) F(E), \\
 M_{33} &= \frac{2}{\hbar k_B T} \int_{-\infty}^{\infty} dE (E - \mu)^2 \sum_{i \neq L} \mathcal{T}_{Li}(E) F(E).
 \end{aligned}$$

where $F(E) \equiv \{4 \cosh^2[(E - \mu)/k_B T]\}^{-1}$. The transmission probability $\mathcal{T}_{ij}(E)$ is calculated using the Caroli formula [1]

$$\mathcal{T}_{ij} = \text{Tr}[\Gamma_i(E) G(E) \Gamma_j(E) G^\dagger(E)], \quad (35)$$

where the (retarded) Green's function for the triple-QD system is $G(E) \equiv (E - H_{\text{qd}} - i\Gamma/2)^{-1}$. The rate for electrons to tunnel from a QD to the nearby electrode, $\Gamma = 2\pi \sum_k |V_{ik}|^2 \delta(\omega - \varepsilon_{ik})$, is assumed to be an identical constant for all three QDs (i.e., Γ does not depend on electronic energy). When an external magnetic flux Φ is applied to the system, the transport coefficients satisfy the Onsager-Casimir relation [1,65]

$$M_{ij}(\phi) = M_{ji}(-\phi), \quad \forall i, j. \quad (36)$$

Using the above equations, we calculate the linear-transport coefficients M_{ij} for a set of physical parameters that define a three-terminal thermoelectric heat engine, i.e., E_i ($i = 1, 2, 3$), Γ , ϕ , t , and T . Throughout this paper we set the equilibrium chemical potential as $\mu = 0$, since tuning the chemical potential is equivalent to tuning the QDs' energy. For each thermoelectric heat engine, we then obtain the dimensionless parameters λ_i ($i = 1, 2, 3$) from the linear-transport coefficients M_{ij} . From the quantities λ_i ($i = 1, 2, 3$), we can obtain the output power [up to W_0 , see Eq. (19)] and the energy efficiency at two working conditions: (i) the maximal energy efficiency condition and (ii) the maximal output power condition. The numerical results are presented graphically in Figs. 4 and 5.

From Fig. 4, one can see that the magnetic flux has only a weak effect on the dimensionless quantities λ_i ($i = 1, 2, 3$) for the model and the parameters we adopted. The dependence on the QD energy E_1 , on the other hand, is much more pronounced. The deviation from the limit where $\lambda_3^2 = \lambda_1 \lambda_2$ (mainly driven by time-reversal symmetry breaking at finite magnetic flux) is not pronounced as well. Consistently, we find from Fig. 5 that the energy efficiency and output power also have a weak dependence on the magnetic flux but a very strong dependence on the QD energy E_1 . Interestingly, for the parameters we adopted, the energy efficiency and output power are high when the magnetic flux is $\phi \approx 0$ and $E_1 \approx 2k_B T$. In such a regime, an appealing energy efficiency, $\eta_{\text{max}} \simeq 0.6\eta_C$, and the efficiency at the maximal output power, $\eta(W_{\text{max}}) \simeq 0.4\eta_C$, can be obtained.

In Figs. 6 and 7, we compare the performance of our setup with the previous setup $P = 0$ for the same three-terminal

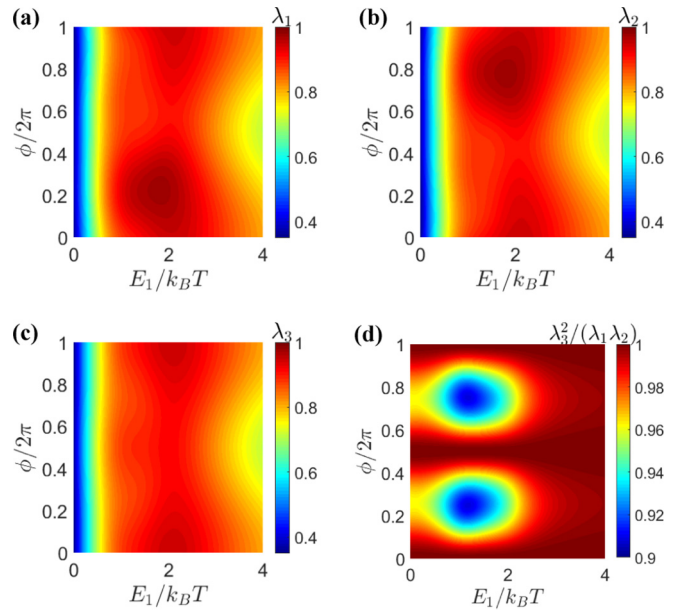


FIG. 4. The dimensionless quantities (a) λ_1 , (b) λ_2 , (c) λ_3 , and (d) $\lambda_3^2/(\lambda_1 \lambda_2)$ as functions of the QD energy E_1 and the magnetic flux ϕ . The other parameters are $t = 0.2k_B T$, $\Gamma = 0.5k_B T$, $\mu = 0$, $E_2 = 1.0k_B T$, and $E_3 = 2.0k_B T$.

quantum-dot heat engine [i.e., the physical parameters E_i ($i = 1, 2, 3$), Γ , μ , t , T , and ϕ are identical for the two setups]. The $P = 0$ setup is illustrated in Fig. 6(a), where the heat and electric currents flowing out of the P terminal vanish by adjusting the electrochemical potential μ_P and temperature T_P of the P terminal. In the $P = 0$ limit, there is only one electric and one heat current, where the maximum energy efficiency and

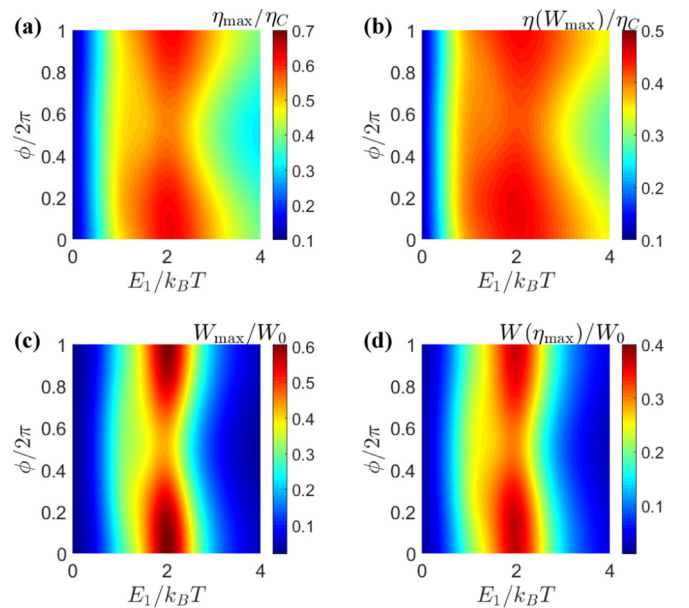


FIG. 5. Maximum energy efficiency and output power in a triple-QD thermoelectric engine. (a) η_{max} , (b) $\eta(W_{\text{max}})$, (c) W_{max} , and (d) $W(\eta_{\text{max}})$ as the functions of the QD energy E_1 and the magnetic flux ϕ . The other parameters are $t = 0.2k_B T$, $\Gamma = 0.5k_B T$, $\mu = 0$, $E_2 = 1.0k_B T$, and $E_3 = 2.0k_B T$.

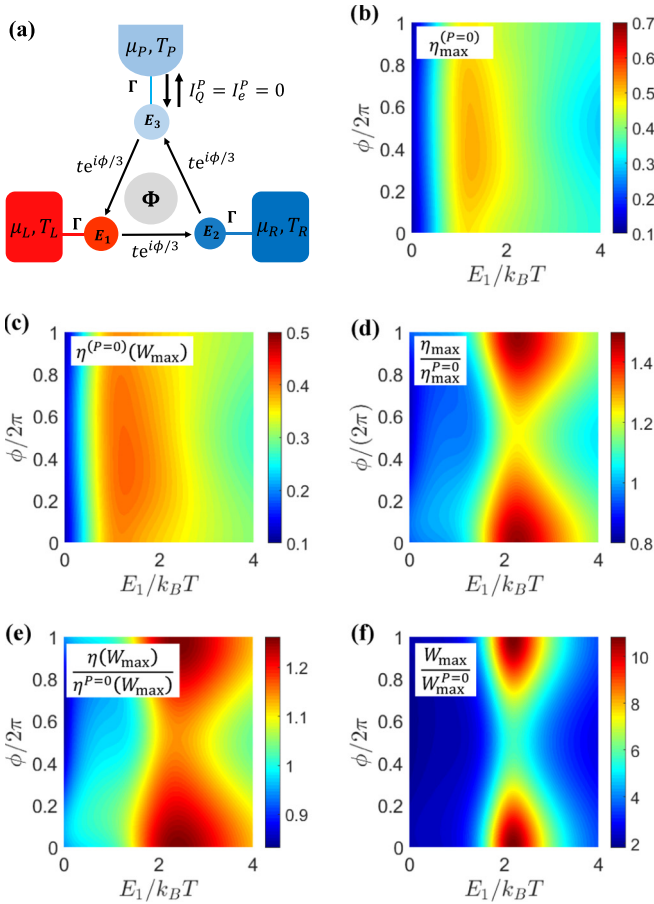


FIG. 6. (a) Schematic of the triple-QD thermoelectric engine when the electric current I_e^p and heat current I_Q^p vanish (denoted as $P = 0$ briefly). (b) The maximum efficiency and (c) the efficiency at maximum power for the $P = 0$ limit as functions of QD energy E_1 and magnetic flux ϕ . (d)–(f) Comparing the maximal energy efficiency and output power for the $P = 0$ limit and the case with two output electric currents for the QD energy E_1 and the magnetic flux ϕ : (d) Maximal efficiency, (e) efficiency at maximum power, and (f) maximum output power. The other parameters are $t = 0.2k_B T$, $\mu = 0$, $E_2 = 1.0k_B T$, and $E_3 = 2.0k_B T$.

output power have been studied in detail before [6,27,49–54]. We emphasize that the $P = 0$ setup has only one output electric current and is thus quite different from our setups. A comparison between them must be interpreted as follows: When the temperatures of the hot and cold reservoirs are set, and the structure of the three-terminal system is given as well, one can choose our setup or the $P = 0$ setup (if T_P can be adjusted) to exploit the thermal energy to gain electric energy. One then chooses between the two setups for better energy efficiency or output power. In the comparison, one must also understand that the gained electric energy may be stored or consumed in different ways for the two setups (the consumption of the gained electric power in our setup will be discussed in detail at the end of this section). As shown in Fig. 6, the maximal efficiency, the efficiency at maximum power, and the maximum output power can be significantly improved when the three-terminal device goes from the $P = 0$ setup to our setup. The improvement is especially pronounced when $\phi \simeq 0$

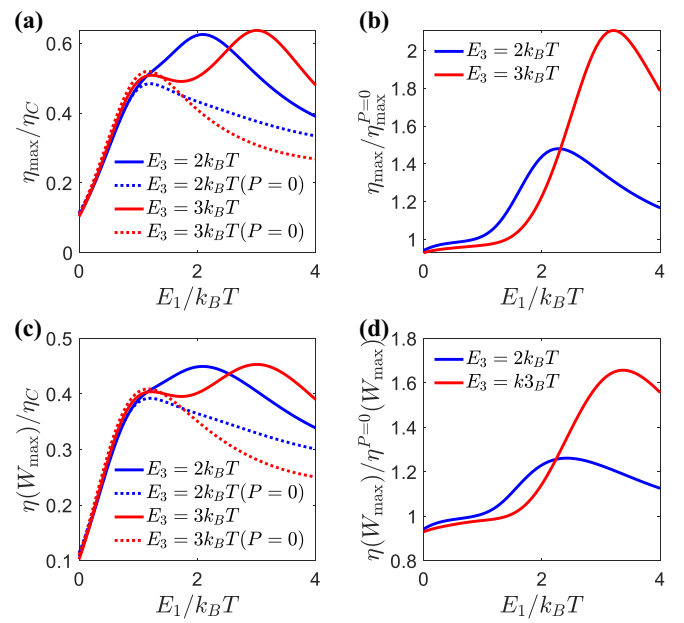


FIG. 7. (a) The maximum efficiency and (c) efficiency at maximum power as functions of E_1 for different E_3 . Comparing the maximal energy efficiency and output power for the $P = 0$ limit and the case with two output electric currents for various QD energies E_1 for different E_3 : (b) Maximal efficiency, and (d) efficiency at maximum power. The other parameters are $t = 0.2k_B T$, $\mu = 0$, $\phi = 0$, and $E_2 = 1.0k_B T$.

and $E_1 \simeq 2k_B T$. In particular, the maximum output power is substantially increased by an order of magnitude when our setup is adopted. We remark that, unlike the $P = 0$ setup where the energy efficiency and output power are improved by introducing the magnetic flux ϕ [49–54], in our setup the $\phi = 0$ limit is favorable for high thermoelectric performance.

We then compare the thermoelectric performance between the $P = 0$ setup and our setup in more detail for the non-magnetic situations with $\phi = 0$. Figure 7(a) shows the maximum energy efficiency for the two setups for two cases: (i) $E_3 = 2k_B T$ and (ii) $E_3 = 3k_B T$. It is seen that for case (i), the maximal energy efficiency for our setup can reach to slightly larger than $0.6\eta_C$, whereas the maximal energy efficiency for the $P = 0$ setup is smaller than $0.5\eta_C$. For case (ii), the maximal energy efficiency for our setup is also considerably larger than the maximal energy efficiency for the $P = 0$ setup. For both cases, the energy efficiency achieved with our setup is very high, $\gtrsim 0.6\eta_C$. Figure 7(b) shows the ratio between the maximal energy efficiency obtained in our setup to that obtained in the $P = 0$ setup. For case (i) this ratio is largest when $E_1 \simeq 2k_B T$, while for case (ii) the ratio is largest when $E_1 \simeq 3.2k_B T$. Similar behaviors are found for the energy efficiency at the maximum output power, as shown in Figs. 7(c) and 7(d). These results demonstrate concretely that our setup may yield considerably better energy efficiency than the $P = 0$ setup, even in the regime where the $P = 0$ setup already has high-energy efficiency. Moreover, comparing Figs. 5(a) and 5(b) and Figs. 6(b) and 6(c), one finds that our setup can substantially increase the physical parameter region with high-energy efficiency. To be more

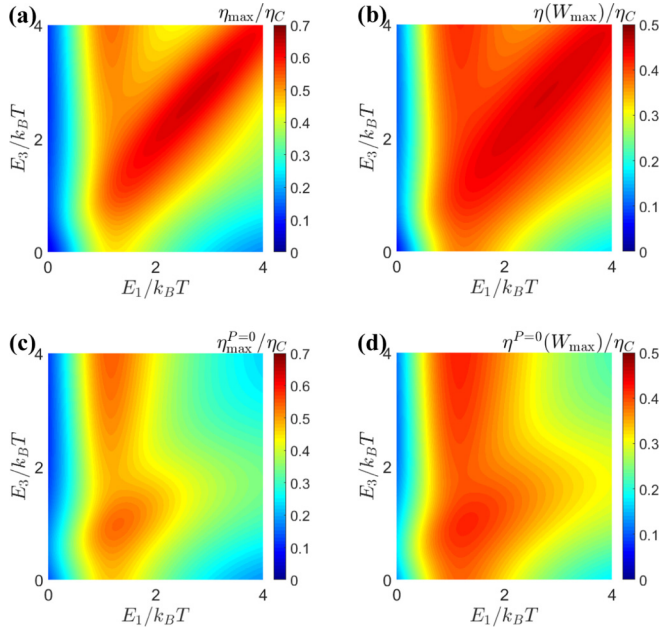


FIG. 8. The maximum efficiency η_{\max} [(a) and (c)] and the efficiency at maximum power $\eta(W_{\max})$ [(b) and (d)] for our setup with two output electric currents [(a) and (b)] and for the $P = 0$ setup [(c) and (d)] as functions of E_1 and E_3 . Other physical parameters are $t = 0.2k_B T$, $\mu = 0$, $\phi = 0$, and $E_2 = 1.0k_B T$. The scales of the color bar are identical for (a) and (c) [(b) and (d)].

careful in this conclusion, we present the maximum energy efficiency and the energy efficiency at maximum power as functions of E_1 and E_3 for both setups in Fig. 8, where we obtain the same conclusion. Importantly, this conclusion implies that for experimental realizations, particularly when the physical parameters cannot be controlled precisely, our setup may have a better chance to yield thermoelectric devices with high-energy efficiency. Indeed, mesoscopic systems have considerable fluctuations where the physical parameters such as the quantum-dot energy cannot be fully controlled in experiments. An enlarged parameter region for high efficiency will increase the feasibility of high-performance mesoscopic thermoelectric devices.

From the above results, we find that the zero magnetic flux cases are favorable for high-performance thermoelectric devices for our setup. This nonmagnetic limit is more appealing for experimental realization and potential applications. In fact, this limit also makes the theory much easier: When $\phi = 0$, $\mathcal{M}_{eQ} = \mathcal{M}_{Qe}^T$, and thus $\lambda_1 = \lambda_2 = \lambda_3$. The maximal energy efficiency can come back to the conventional form of

$$\eta_{\max} = \eta_C \frac{\sqrt{ZT+1} - 1}{\sqrt{ZT+1} + 1}, \quad ZT = \frac{\lambda_3}{1 - \lambda_3}. \quad (37)$$

We now discuss the practical problem of connecting the three-terminal thermoelectric heat engine to a resistor circuit which receives the electric power. According to Ref. [8], the best performance of the engine-resistor system is given by the impedance matching between the engine and the resistor. For the three-terminal setup, we shall use a triangular resistor circuit to receive the electric power to achieve the best performance, as schematically shown in Fig. 9. For simplicity,

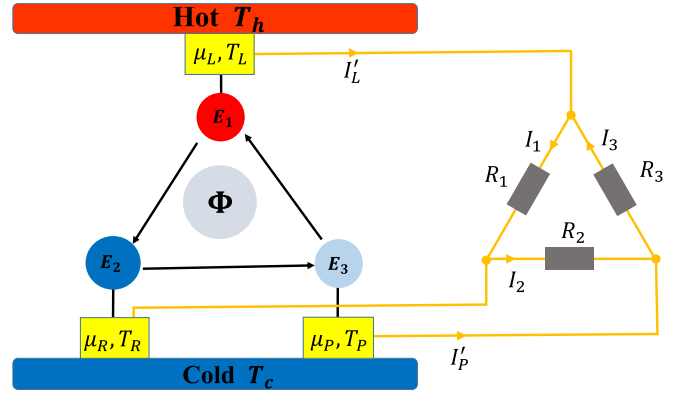


FIG. 9. The three-terminal thermoelectric device is connected with a three-resistor circuit, where the resistors (denoted as R_i , $i = 1, 2, 3$) are connected to three electrodes, and I_i represents the current following through each resistor.

this discussion will be restricted to the time-reversal symmetric limit. The current-force response matrix for the resistor circuit is

$$\vec{I}'_e = \hat{\mathcal{M}}_L \vec{F}'_e, \quad (38)$$

where $\vec{I}'_e = (I'_L, I'_P)^T$. I'_L and I'_P are electric currents following from L and P electrodes into the resistor circuit, respectively. The electric currents following through the resistors R_i ($i = 1, 2, 3$) are given by

$$I_1 = \frac{\mu_L - \mu_R}{eR_1} = \frac{F_e^L}{R_1}, \quad (39a)$$

$$I_2 = \frac{\mu_R - \mu_P}{eR_2} = -\frac{F_e^P}{R_2}, \quad (39b)$$

$$I_3 = \frac{\mu_P - \mu_L}{eR_3} = \frac{F_e^P - F_e^L}{R_3}. \quad (39c)$$

On one hand, using Kirchhoff's current law for the resistor circuit, we obtain

$$\begin{aligned} I'_L - I_1 + I_3 &= 0, \\ I'_P + I_2 - I_3 &= 0. \end{aligned} \quad (40)$$

Combining Eqs. (38)–(40), we arrive at the expression for $\hat{\mathcal{M}}_L$,

$$\hat{\mathcal{M}}_L = \begin{pmatrix} \frac{1}{R_1} + \frac{1}{R_3} & -\frac{1}{R_3} \\ -\frac{1}{R_3} & \frac{1}{R_2} + \frac{1}{R_3} \end{pmatrix}. \quad (41)$$

On the other hand, Kirchhoff's current law for the electrodes requires that

$$\vec{I}'_e + \vec{I}_e = 0. \quad (42)$$

Therefore,

$$\vec{F}'_e = -(\hat{\mathcal{M}}_{ee} + \hat{\mathcal{M}}_L)^{-1} \hat{\mathcal{M}}_{eQ} F_Q. \quad (43)$$

The power consumed by the resistor circuit is then

$$\begin{aligned} W &= \vec{F}'_e{}^T \hat{\mathcal{M}}_L \vec{F}'_e \\ &= \hat{\mathcal{M}}_{Qe} (\hat{\mathcal{M}}_{ee} + \hat{\mathcal{M}}_L)^{-1} \hat{\mathcal{M}}_L (\hat{\mathcal{M}}_{ee} + \hat{\mathcal{M}}_L)^{-1} \hat{\mathcal{M}}_{eQ} F_Q^2. \end{aligned} \quad (44)$$

The input heat current is given by

$$I_Q = [-\hat{\mathcal{M}}_{Qe}(\hat{\mathcal{M}}_{ee} + \hat{\mathcal{M}}_L)^{-1}\hat{\mathcal{M}}_{eQ} + \mathcal{M}_{QQ}]F_Q. \quad (45)$$

The energy efficiency is then given by $\eta = W/I_Q$. By varying $\hat{\mathcal{M}}_L$, we find that the maximum output power is reached at

$$\hat{\mathcal{M}}_L = \hat{\mathcal{M}}_{ee}, \quad (46)$$

whereas the maximum energy efficiency is reached at

$$\hat{\mathcal{M}}_L = \sqrt{1 - \lambda_3}\hat{\mathcal{M}}_{ee}. \quad (47)$$

The energy efficiency and output power for these two conditions are the same as what we obtained before, in Eqs. (17), (19), (21), and (22).

VI. CONCLUSION AND DISCUSSIONS

In conclusion, we study the thermoelectric performance of a three-terminal quantum-dot heat engine in a setup with two output electric currents. We derive the formulas for the maximum energy efficiency and output power, as well as their

trade-off. With such a formulation, we calculate the maximum efficiency and power for various physical parameters of the quantum-dot three-terminal thermoelectric engine. Through concrete numerical results, we find that the setup with two output electric currents can substantially enlarge the parameter region with high efficiency and power, and thus provides a promising pathway toward high-performance thermoelectric devices. These results introduce intriguing features on thermoelectric energy conversion in the mesoscopic regime, with particular emphasis on multiterminal setups with multiple output electric currents. Our study indicates that such setups, though having been ignored before, can be promising for high-performance thermoelectric energy conversion.

ACKNOWLEDGMENTS

J.L., Y.L., R.W., and J.-H.J. acknowledge support from the National Natural Science Foundation of China (NSFC Grant No. 11675116) and a Project Funded by the Priority Academic Program Development of Jiangsu Higher Education Institutions (PAPD). C.W. is supported by the National Natural Science Foundation of China under Grant No. 11704093.

-
- [1] P. N. Butcher, Thermal and electrical transport formalism for electronic microstructures with many terminals, *J. Phys.: Condens. Matter* **2**, 4869 (1990).
 - [2] Y. Dubi and M. Di Ventra, Heat flow and thermoelectricity in atomic and molecular junctions, *Rev. Mod. Phys.* **83**, 131 (2011).
 - [3] N. Li, J. Ren, L. Wang, G. Zhang, P. Hänggi, and B. Li, Phononics: Manipulating heat flow with electronic analogs and beyond, *Rev. Mod. Phys.* **84**, 1045 (2012).
 - [4] B. Sothmann, R. Sánchez, and A. N. Jordan, Thermoelectric energy harvesting with quantum dots, *Nanotechnology* **26**, 032001 (2015).
 - [5] J.-H. Jiang and Y. Imry, Linear and nonlinear mesoscopic thermoelectric transport with coupling with heat baths, *C. R. Phys.* **17**, 1047 (2016).
 - [6] G. Benenti, G. Casati, K. Saito, and R. S. Whitney, Fundamental aspects of steady-state conversion of heat to work at the nanoscale, *Phys. Rep.* **694**, 1 (2017).
 - [7] O. Entin-Wohlman, J.-H. Jiang, and Y. Imry, Efficiency and dissipation in a two-terminal thermoelectric junction, emphasizing small dissipation, *Phys. Rev. E* **89**, 012123 (2014).
 - [8] J.-H. Jiang, Thermodynamic bounds and general properties of optimal efficiency and power in linear responses, *Phys. Rev. E* **90**, 042126 (2014).
 - [9] R. S. Whitney, Most Efficient Quantum Thermoelectric at Finite Power Output, *Phys. Rev. Lett.* **112**, 130601 (2014).
 - [10] R. S. Whitney, Finding the quantum thermoelectric with maximal efficiency and minimal entropy production at given power output, *Phys. Rev. B* **91**, 115425 (2015).
 - [11] G. Verley, M. Esposito, T. Willaert, and C. Van den Broeck, The unlikely Carnot efficiency, *Nat. Commun.* **5**, 4721 (2014).
 - [12] M. Polettini, G. Verley, and M. Esposito, Efficiency Statistics at All Times: Carnot Limit at Finite Power, *Phys. Rev. Lett.* **114**, 050601 (2015).
 - [13] J.-H. Jiang, B. K. Agarwalla, and D. Segal, Efficiency Statistics and Bounds for Systems with Broken Time-Reversal Symmetry, *Phys. Rev. Lett.* **115**, 040601 (2015).
 - [14] M. Bauer, K. Brandner, and U. Seifert, Optimal performance of periodically driven, stochastic heat engines under limited control, *Phys. Rev. E* **93**, 042112 (2016).
 - [15] K. Proesmans, Y. Dreher, M. Gavrilov, J. Bechhoefer, and C. Van den Broeck, Brownian Duet: A Novel Tale of Thermodynamic Efficiency, *Phys. Rev. X* **6**, 041010 (2016).
 - [16] K. Proesmans, B. Cleuren, and C. Van den Broeck, Power-Efficiency-Dissipation Relations in Linear Thermodynamics, *Phys. Rev. Lett.* **116**, 220601 (2016).
 - [17] P. Pietzonka and U. Seifert, Universal Trade-off between Power, Efficiency, and Constancy in Steady-State Heat Engines, *Phys. Rev. Lett.* **120**, 190602 (2018).
 - [18] D. Sánchez and L. Serra, Thermoelectric transport of mesoscopic conductors coupled to voltage and thermal probes, *Phys. Rev. B* **84**, 201307(R) (2011).
 - [19] R. Sánchez and M. Büttiker, Optimal energy quanta to current conversion, *Phys. Rev. B* **83**, 085428 (2011).
 - [20] J.-H. Jiang, O. Entin-Wohlman, and Y. Imry, Thermoelectric three-terminal hopping transport through one-dimensional nanosystems, *Phys. Rev. B* **85**, 075412 (2012).
 - [21] B. Sothmann, R. Sánchez, A. N. Jordan, and M. Büttiker, Rectification of thermal fluctuations in a chaotic cavity heat engine, *Phys. Rev. B* **85**, 205301 (2012).
 - [22] J.-H. Jiang, O. Entin-Wohlman, and Y. Imry, Hopping thermoelectric transport in finite systems: Boundary effects, *Phys. Rev. B* **87**, 205420 (2013).
 - [23] L. Simine and D. Segal, Path-integral simulations with fermionic and bosonic reservoirs: Transport and dissipation in molecular electronic junctions, *J. Chem. Phys.* **138**, 214111 (2013).

- [24] B. Sothmann, R. Sánchez, A. N. Jordan, and M. Büttiker, Powerful energy harvester based on resonant-tunneling quantum wells, *New J. Phys.* **15**, 095021 (2013).
- [25] J.-H. Jiang, O. Entin-Wohlman, and Y. Imry, Three-terminal semiconductor junction thermoelectric devices: Improving performance, *New J. Phys.* **15**, 075021 (2013).
- [26] F. Mazza, S. Valentini, R. Bosisio, G. Benenti, V. Giovannetti, R. Fazio, and F. Taddei, Separation of heat and charge currents for boosted thermoelectric conversion, *Phys. Rev. B* **91**, 245435 (2015).
- [27] R. S. Whitney, Quantum coherent three-terminal thermoelectrics: Maximum efficiency at given power output, *Entropy* **18**, 208 (2016).
- [28] M. Campisi and R. Fazio, The power of a critical heat engine, *Nat. Commun.* **7**, 11895 (2016).
- [29] K. Brandner and U. Seifert, Multi-terminal thermoelectric transport in a magnetic field: Bounds on Onsager coefficients and efficiency, *New J. Phys.* **15**, 105003 (2013).
- [30] B. K. Agarwalla, J.-H. Jiang, and D. Segal, Full counting statistics of vibrationally assisted electronic conduction: Transport and fluctuations of thermoelectric efficiency, *Phys. Rev. B* **92**, 245418 (2015).
- [31] L. Li and J.-H. Jiang, Staircase quantum dots configuration in nanowires for optimized thermoelectric power, *Sci. Rep.* **6**, 31974 (2016).
- [32] K. Yamamoto, O. Entin-Wohlman, A. Aharony, and N. Hatano, Efficiency bounds on thermoelectric transport in magnetic fields: The role of inelastic processes, *Phys. Rev. B* **94**, 121402(R) (2016).
- [33] B. K. Agarwalla, J.-H. Jiang, and D. Segal, Quantum efficiency bound for continuous heat engines coupled to noncanonical reservoirs, *Phys. Rev. B* **96**, 104304 (2017).
- [34] K. Macieszczak, K. Brandner, and J. P. Garrahan, Unified Thermodynamic Uncertainty Relations in Linear Response, *Phys. Rev. Lett.* **121**, 130601 (2018).
- [35] J.-H. Jiang and Y. Imry, Near-field three-terminal thermoelectric heat engine, *Phys. Rev. B* **97**, 125422 (2018).
- [36] O. Entin-Wohlman, Y. Imry, and A. Aharony, Enhanced performance of joint cooling and energy production, *Phys. Rev. B* **91**, 054302 (2015).
- [37] J. Lu, R. Wang, J. Ren, M. Kulkarni, and J.-H. Jiang, Quantum-dot circuit-QED thermoelectric diodes and transistors, *Phys. Rev. B* **99**, 035129 (2019).
- [38] S.-Y. Hwang, D. Sánchez, M. Lee, and R. López, Magnetic-field asymmetry of nonlinear thermoelectric and heat transport, *New J. Phys.* **15**, 105012 (2013).
- [39] J. Matthews, F. Battista, D. Sánchez, P. Samuelsson, and H. Linke, Experimental verification of reciprocity relations in quantum thermoelectric transport, *Phys. Rev. B* **90**, 165428 (2014).
- [40] H. Thierschmann, R. Sánchez, B. Sothmann, F. Arnold, C. Heyn, W. Hansen, H. Buhmann, and L. W. Molenkamp, Three-terminal energy harvester with coupled quantum dots, *Nat. Nanotech.* **10**, 854 (2015).
- [41] B. Roche, P. Roulleau, T. Jullien, Y. Jompol, I. Farrer, D. A. Ritchie, and D. C. Glatthli, Harvesting dissipated energy with a mesoscopic ratchet, *Nat. Commun.* **6**, 6738 (2015).
- [42] L. Cui, R. Miao, K. Wang, D. Thompson, L. A. Zotti, J. C. Cuevas, E. Meyhofer, and P. Reddy, Peltier cooling in molecular junctions, *Nat. Nanotechnol.* **13**, 122 (2018).
- [43] T. E. Humphrey, R. Newbury, R. P. Taylor, and H. Linke, Reversible Quantum Brownian Heat Engines for Electrons, *Phys. Rev. Lett.* **89**, 116801 (2002).
- [44] T. E. Humphrey and H. Linke, Reversible Thermoelectric Nanomaterials, *Phys. Rev. Lett.* **94**, 096601 (2005).
- [45] I. Iyyappan and M. Ponnuragan, General relations between the power, efficiency, and dissipation for the irreversible heat engines in the nonlinear response regime, *Phys. Rev. E* **97**, 012141 (2018).
- [46] J.-H. Jiang, Enhancing efficiency and power of quantum-dots resonant tunneling thermoelectrics in three-terminal geometry by cooperative effects, *J. Appl. Phys.* **116**, 194303 (2014).
- [47] J. Lu, R. Wang, Y. Liu, and J.-H. Jiang, Thermoelectric cooperative effect in three-terminal elastic transport through a quantum dot, *J. Appl. Phys.* **122**, 044301 (2017).
- [48] J.-H. Jiang and Y. Imry, Enhancing Thermoelectric Performance Using Nonlinear Transport Effects, *Phys. Rev. Applied* **7**, 064001 (2017).
- [49] G. Benenti, K. Saito, and G. Casati, Thermodynamic Bounds on Efficiency for Systems with Broken Time-Reversal Symmetry, *Phys. Rev. Lett.* **106**, 230602 (2011).
- [50] K. Brandner, K. Saito, and U. Seifert, Strong Bounds on Onsager Coefficients and Efficiency for Three-Terminal Thermoelectric Transport in A Magnetic Field, *Phys. Rev. Lett.* **110**, 070603 (2013).
- [51] K. Saito, G. Benenti, G. Casati, and T. Prosen, Thermopower with broken time-reversal symmetry, *Phys. Rev. B* **84**, 201306(R) (2011).
- [52] V. Balachandran, G. Benenti, and G. Casati, Efficiency of three-terminal thermoelectric transport under broken time-reversal symmetry, *Phys. Rev. B* **87**, 165419 (2013).
- [53] K. Brandner and U. Seifert, Bound on thermoelectric power in a magnetic field within linear response, *Phys. Rev. E* **91**, 012121 (2015).
- [54] J. Stark, K. Brandner, K. Saito, and U. Seifert, Classical Nernst Engine, *Phys. Rev. Lett.* **112**, 140601 (2014).
- [55] F. Mazza, R. Bosisio, G. Benenti, V. Giovannetti, R. Fazio, and F. Taddei, Thermoelectric efficiency of three-terminal quantum thermal machines, *New J. Phys.* **16**, 085001 (2014).
- [56] F. L. Curzon and B. Ahlborn, Efficiency of a Carnot engine at maximum power output, *Am. J. Phys.* **43**, 22 (1975).
- [57] C. Van den Broeck, Thermodynamic Efficiency at Maximum Power, *Phys. Rev. Lett.* **95**, 190602 (2005).
- [58] N. Golubeva and A. Imparato, Efficiency at Maximum Power of Interacting Molecular Machines, *Phys. Rev. Lett.* **109**, 190602 (2012).
- [59] N. Shiraishi, K. Saito, and H. Tasaki, Universal Trade-off Relation between Power and Efficiency for Heat Engines, *Phys. Rev. Lett.* **117**, 190601 (2016).
- [60] O. Raz, Y. Subaşı, and R. Pugatch, Geometric Heat Engines Featuring Power that Grows with Efficiency, *Phys. Rev. Lett.* **116**, 160601 (2016).
- [61] A. E. Allahverdyan, K. V. Hovhannissyan, A. V. Melkikh, and S. G. Gevorgian, Carnot Cycle at Finite Power: Attainability of Maximal Efficiency, *Phys. Rev. Lett.* **111**, 050601 (2013).
- [62] G. Benenti, G. Casati, and J. Wang, Conservation Laws and Thermodynamic Efficiencies, *Phys. Rev. Lett.* **110**, 070604 (2013).

- [63] V. Holubec and A. Ryabov, Cycling Times Power Fluctuations Near Optimum Efficiency, [Phys. Rev. Lett. **121**, 120601 \(2018\)](#).
- [64] U. Seifert, Stochastic thermodynamics, fluctuation theorems and molecular machines, [Rep. Prog. Phys. **75**, 126001 \(2012\)](#).
- [65] U. Sivan and Y. Imry, Multichannel Landauer formula for thermoelectric transport with application to thermopower near the mobility edge, [Phys. Rev. B **33**, 551 \(1986\)](#).